Chemical Science

EDGE ARTICLE

View Article Online
View Journal | View Issue

Cite this: *Chem. Sci.*, 2020, **11**, 281

All publication charges for this article have been paid for by the Royal Society of Chemistry

Physicochemical-property guided design of a highly sensitive probe to image nitrosative stress in the pathology of stroke†

Juan Cheng,‡[a] Dan Li,‡[a] Meiling Sun,‡[b] Yi Wang,[c] Qiao-Qin Xu,[a] Xing-Guang Liang,[ac] Yun-Bi Lu,[c] Yongzhou Hu,[a] Feng Han*[b] and Xin Li*[a]

In vivo real-time imaging of nitrosative stress in the pathology of stroke has long been a formidable challenge due to both the presence of the blood–brain barrier (BBB) and the elusive nature of reactive nitrogen species, while this task is also informative to gain a molecular level understanding of neurovascular injury caused by nitrosative stress during the stroke episode. Herein, using a physicochemical property-guided probe design strategy in combination with the reaction-based probe design rationale, we have developed an ultrasensitive probe for imaging nitrosative stress evolved in the pathology of stroke. This probe demonstrates an almost zero background fluorescence signal but a maximum 1000-fold fluorescence enhancement in response to peroxynitrite, the nitrosative stress marker. Due to its good physicochemical properties, the probe readily penetrates the BBB after intravenous administration, and quickly accumulates in mice brain to sense local vascular injuries. After accomplishing its imaging mission, the probe is easily metabolized and therefore won't cause safety concerns. These desirable features make the probe competent for the straightforward visualization of nitrosative stress progression in stroke pathology.

Received 31st July 2019
Accepted 8th November 2019

DOI: 10.1039/c9sc03798e

rsc.li/chemical-science

Stroke is an acute episode of focal dysfunction of the brain, spinal cord or retina lasting longer than 24 h.[1] It is one of the most dangerous diseases with a high rate of mortality and disability. Despite recent remarkable advances in its treatment and prevention, stroke remains the second single most frequent cause of death for people older than 60 years and the first cause of permanent disability.[2] With the aging of the world's population, the global burden of stroke keeps increasing. In consequence, there is a pressing need to continue investigating the mechanism, prevention and treatment of this devastating disease. Several key players contribute to neuronal injury and death following stroke, including oxidative and nitrosative stress, excitotoxicity, and inflammation,[3] among which, the damaging role of nitrosative stress is attracting increasing research interest. Nitrosative stress is represented by the overproduction of peroxynitrite ($ONOO^-$) during both cerebral ischemia and subsequent reperfusion.[4,5] It facilitates the demise of the penumbra by protein nitration, lipid peroxidation, DNA oxidation, mitochondrial damage, activation or inhibition of various signaling pathways, and blood–brain barrier (BBB) breakdown.[6] Due to its ultrahigh toxicity, it is emerging as an attractive molecular target for therapeutic intervention.[6]

One of the main challenges in the development of $ONOO^-$-targeted stroke treatment is the ideal timing and dosage of medication, as this determines a lot of clinical outcomes.[7] A technology capable of spatiotemporally mapping nitrosative stress during stroke onset and progression would improve people's understanding of when and how $ONOO^-$ overproduction contributes to stroke pathology, yielding straightforward information for treatment design. However, this has long been a forbidden task due to the extremely short half-life of $ONOO^-$ and its non-genetic origin.[8,9] Recent advances in reaction-based small-molecule fluorescent probes provide the possibility to track elusive small biomolecules in their local environments.[10,11] Actually, for targeting $ONOO^-$, there have been several robust probes reported that were confirmed for their specificity and capability to image nitrosative stress in the context of inflammation,[12–16] kidney injury,[17] hepatotoxicity,[18–21] and heart disease.[22,23] However, the context of the neurovascular unit is more formidable due to the presence of the blood–brain barrier (BBB). Actually, due to the rigid planar structure of most fluorophores which is essential for their emissive properties, few probes have been reported to readily penetrate the BBB and

[a]College of Pharmaceutical Sciences, Zhejiang University, Hangzhou 310058, China. E-mail: lixin81@zju.edu.cn

[b]School of Pharmacy, Nanjing Medical University, Nanjing 211166, China. E-mail: fenghan169@njmu.edu.cn

[c]School of Medicine, Zhejiang University, Hangzhou 310058, China

† Electronic supplementary information (ESI) available. See DOI: 10.1039/c9sc03798e

‡ These authors contributed equally to this work.

realize the non-invasive imaging of stroke events. Herein, we reported our physicochemical-property guided design of an ultrasensitive fluorogenic probe, which demonstrates desirable brain distribution after intravenous injection to fulfill the direct observation of nitrosative stress during stroke onset and progression.

Results and discussion

Physicochemical-property guided probe design

To image local nitrosative stress during stroke onset, it is necessary for the probe to readily penetrate the BBB and accumulate there to a desirable concentration. Similar to the principles in drug development, we assume that the physicochemical properties of a probe should play a key role in determining its *in vivo* absorption and distribution properties. To rationally design a probe with promising brain absorption and distribution properties, we screened a set of classical fluorescent dyes with sufficient brightness for their partition coefficient between water and oil (log *P*), which is the fundamental principle for BBB permeability (Fig. 1a).[24] Log *P* measurements were conducted with a shake flask *n*-octanol/water partition experiment. The results showed that among the eight fluorophores commonly used for bio-imaging (Fig. S1†), the benzo-BODIPY scaffold (**F4**) showed a log *P* of 2.60 which falls into the suggested threshold of 2–5 proposed by Hitchcock *et al.* for possible BBB permeability (Fig. 1a).[24] Moreover, **F4** also demonstrated a moderate water solubility of 250 μM as determined by the UV-Visible spectrophotometric method (Fig. S2†). Besides, **F4** was quite bright with a quantum yield (Φ) of 0.788 in aqueous solution. All these physicochemical and photophysical properties make the **F4** fluorophore a desirable starting point for probe development.

Given the reactivity of $ONOO^-$ to oxidize electron-rich phenols into quinines which has been utilized with a high degree of success for $ONOO^-$ probe design (Fig. 1b),[25–30] the *p*-hydroxyl aniline moiety was selected as a reaction trigger for $ONOO^-$ sensing, and probes **B545a** and **B545b** were designed (Fig. 1c). We envisioned that probes **B545a** and **B545b** should have little fluorescence due to the free rotation between the fluorophore and the *p*-hydroxyl aniline moiety, while the *p*-hydroxyl aniline moiety should be readily oxidized by $ONOO^-$ under biological conditions, yielding a fluorophore structurally similar to **F4** with strong fluorescence. And this change in probe fluorescence intensity may be recorded as a signal output for $ONOO^-$ sensing.

Probes **B545a** and **B545b** were facilely synthesized by the nucleophilic substitution of α-chloro benzo-BODIPY with the corresponding anilines referring to literature procedures.[31] Their structures were characterized by both NMR spectroscopy and HRMS analysis.

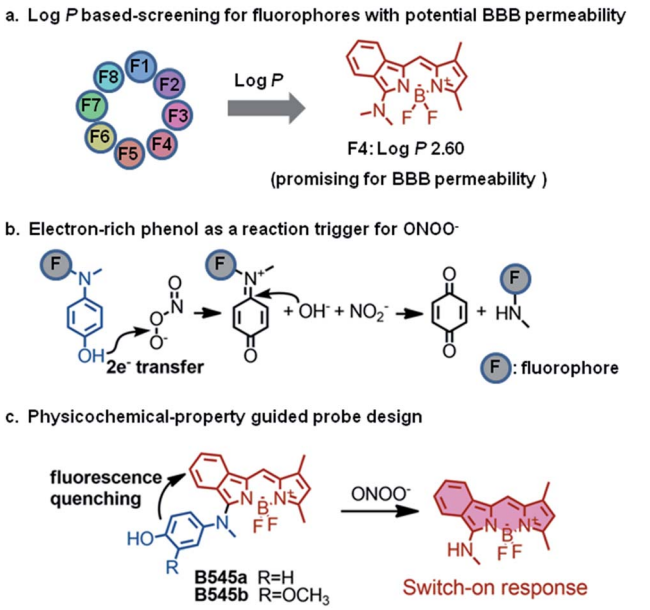

Fig. 1 Physicochemical-property guided fluorescent probe design for non-invasive imaging of $ONOO^-$ during stroke in live mice. (a) Partition coefficients (log *P*) of classical fluorophores were determined and benzo-BODIPY (**F4**) was predicted to have a potentially good BBB permeability. (b) Electron-rich phenols may be oxidized to quinine by $ONOO^-$ and this reaction has been used as a trigger for $ONOO^-$ probe development. (c) Probes **B545a** and **B545b** were designed based on the **F4** fluorophore which showed desirable log *P* for BBB permeability. **B545a** and **B545b** were hypothesized to undergo a biocompatible reaction with $ONOO^-$ to be transformed into highly fluorescent products.

Validating the reactivity of probes B545a and B545b towards $ONOO^-$

Initially, the performance of the two probes in response to $ONOO^-$ was evaluated in PBS buffer (10 mM, pH 7.4). As expected, the probes alone were barely fluorescent (5 μM), presumably due to the energy consumption caused by the free rotation of the phenol ring around the BODIPY ring (Fig. S3a†). However, the addition of $ONOO^-$ (10 μM) triggered almost a simultaneous fluorescence intensity increase of the two probes, with probe **B545b** giving a more dramatic increase (741-fold) than **B545a** (5-fold) (Fig. S3b†). We presume that the better sensitivity of **B545b** is due to the additional methoxyl group *ortho* to the hydroxyl group which is electron-donating and in consequence makes the electron transferring reaction towards $ONOO^-$ more efficient. **B545b** was then selected as a candidate probe for $ONOO^-$ detection and its responsive features were studied in detail under biologically relevant conditions (PBS, 10 mM, pH 7.4).

First, changes in the absorptive spectra of **B545b** in response to various doses of $ONOO^-$ were examined. As shown in Fig. 2a, **B545b** showed its maximum absorption at 508 nm (ε 23 350) attributed to the $\pi \rightarrow \pi^*$ absorption of the BODIPY core. However, the intensity of this band decreased gradually with increasing dose of $ONOO^-$. And a slight blue shift of the maximum absorbance wavelength (498 nm) was observed, suggesting that the benzo-BODIPY scaffold remained largely intact under this condition while the newly formed substitution demonstrated a lower auxochromic effect compared to the *p*-hydroxyl aniline moiety. This observation agrees with the proposed dearylation reaction of **B545b** induced by $ONOO^-$.

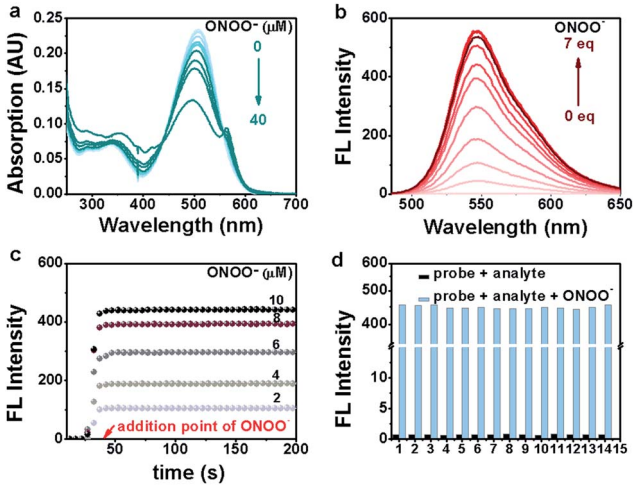

Fig. 2 UV-Vis and fluorescence response of probe **B545b** to $ONOO^-$. (a) Absorption spectra of **B545b** (10.0 μM) before and after being treated with various amounts of $ONOO^-$. (b) Fluorescence spectra of probe **B545b** (5.0 μM) before and after treatment with $ONOO^-$ at indicated final concentrations. (c) Time-lapse emission of **B545b** (5.0 μM) at 545 nm in response to $ONOO^-$. (d) Fluorescence intensity of **B545b** (5.0 μM) at 545 nm after treatment with various biologically related species. (1) Probe blank, (2) NO, (3) NO_2^-, (4) NO_3^- (5) H_2O_2, (6) THBP, (7) $^{\bullet}OH$, (8) $^1O_2$ (9) O_2^-, (10) ClO^-, (11) GSH, (12) Cys, (13) Zn^{2+}, and (14) Cu^{2+}. All analytes were kept at a final concentration of 100 μM except $ONOO^-$ which was kept at 10 μM. All measurements were carried out at ambient temperature with excitation at 475 nm and emission at 545 nm.

Then, the fluorescence titration experiment was performed, and an increase of **B545b** emission intensity was observed after $ONOO^-$ treatment. The increase was $ONOO^-$ dose-dependent (Fig. 2b). Plotting the **B545b** emission intensity at 545 nm *versus* $ONOO^-$ concentration gave an exponential dependence (Fig. S4†), suggesting a positive correlation between the $ONOO^-$ concentration and **B545b** fluorescence intensity. Notably, even a trace amount of $ONOO^-$ as low as 50 nM could still trigger an 8-fold enhancement of **B545b** emission intensity (Fig. S5†). An $ONOO^-$ concentration as low as 0.5 nM can induce a statistically significant increase of **B545b** fluorescence (Fig. S6†). All these results suggest the high sensitivity of **B545b**, supported by both its weak background signal and the high quantum yield of the **F4** fluorophore.

Next, the kinetic properties of the detection reaction were studied. For this purpose, **B545b** fluorescence was recorded in a time-lapsed way before and after $ONOO^-$ treatment. An immediate increase of **B545b** fluorescence was observed as $ONOO^-$ was added, and the increase plateaued in 10 seconds (Fig. 2c), suggesting the ultrafast detection kinetics of **B545b** for $ONOO^-$.

The selectivity of **B545b** for $ONOO^-$ was tested by recording its fluorescence response towards various biologically related species especially reactive oxidative species. It turned out that only $ONOO^-$ could switch on the fluorescence of **B545b** (Fig. 2d). It is noteworthy that **B545b** could still respond to $ONOO^-$ with a similar degree of fluorescence enhancement even in the presence of other biologically related species, suggesting its potential applicability for detecting $ONOO^-$ in a complex environment.

As the H^+ concentration is modestly increased in ischemic tissues in early stages of ischemia as a result of lactic acidosis which leads to a decrease in pH to 6.4–6.7,[32] it is therefore necessary to check the effect of surrounding pH on the detection sensitivity of **B545b**. As shown in Fig. S7,† **B545b** in various pH surroundings responded to a set dose of $ONOO^-$ with a similar degree of fluorescence increase, suggesting that **B545b** should be able to image $ONOO^-$ with a similar degree of sensitivity in the acidified bio-microenvironments.

Finally, after confirming the sensitive and selective fluorescence switch-on response of **B545b** to $ONOO^-$, we monitored the detection reaction with a liquid chromatograph equipped with a mass detector (LC-MS) to make further confirmation on the detection mechanism. Treating **B545b** with $ONOO^-$ caused an $ONOO^-$-dose dependent decrease of the **B545b** signal in the chromatogram while the emergence of a peak whose molecular weight agrees well with the proposed detection product in Fig. 1c (Fig. S8–S10†).

B545b safety and BBB permeability evaluation

Having confirmed the good performance of probe **B545b** as a fluorogenic probe for sensing $ONOO^-$ in aqueous solution, we then tested its cytotoxicity and BBB permeability as a further evaluation of its bio-imaging applicability. With a CCK8 assay, **B545b** was found to cause a negligible effect on the viability of EA.hy926 cells (Fig. S11†), implying its safety for bio-imaging.

The log *P* of **B545b** was measured to be 2.7 by the shake flask *n*-octanol/water partition experiment, which, as expected, falls into the scope of 2–5 proposed by Hitchcock *et al.* for possible BBB permeability.[24] To make further confirmation, the BBB permeability of **B545b** was determined with the classical pharmacokinetic techniques (intravenous administration and tissue sampling).[33] Mice were administered with **B545b** (5 mg kg^{-1}) *via* intravenous injection, and then sacrificed at different time intervals to measure **B545b** concentrations in the brain and plasma. As shown in Fig. S12,† due to its desirable physicochemical properties, **B545b** accumulates easily in the brain tissue, and a brain-to-plasma concentration ratio of 5 was observed in mice 30 min after probe administration. Moreover, **B545b** is easily metabolized. Its plasma and brain concentration dropped significantly in 2 h after administration. This good brain uptake, but non-retention pharmacokinetic properties, of **B545b** is especially desirable, as this should decrease its risk on brain function.

B545b-aided observation of $ONOO^-$ formation in endothelial cells

To test the sensitivity of **B545b** to image $ONOO^-$ in live cells, we first optimized its working concentration for live cell staining. EA.hy926 cells were first treated with 3-morpholinosydnonimine (SIN-1, 0.06 mM), an $ONOO^-$ donor,[34] to up-regulate intracellular $ONOO^-$ levels. After being stained with **B545b** of various concentrations for 30 min, cells were observed under a confocal microscope. The results showed that the intracellular **B545b** fluorescence increased in a probe dose-dependent way,

and significant brightness was observed at a concentration of 0.5 μM (Fig. S13†). Furthermore, **B545b** at 0.5 μM also worked well to image endogenous $ONOO^-$ in cells induced by oxygen-glucose deprivation stimulation (OGD, 4 hours).[35] This suggests that a **B545b** concentration of 0.5 μM should be sufficient for imaging experiments (Fig. S14†).

Then, the capability of **B545b** to image various degrees of nitrosative stress in EA.hy926 cells was studied. Cells were first stimulated with various doses of SIN-1 for 60 min to induce various degrees of nitrosative stress, and then were stained with **B545b** for 30 min. The intracellular **B545b** fluorescence was observed to increase in a SIN-1 dose-dependent way (Fig. 3a and b), indicating the positive correlation between **B545b** fluorescence and the degree of nitrosative stress. It is noteworthy that **B545b** was able to track the dynamic progression of intracellular nitrosative stress induced by SIN-1 stimulation. As shown in Fig. 3c and 3d, when EA.hy926 cells were first loaded with **B545b** (30 min incubation) and then stimulated with SIN-1, the intracellular **B545b** fluorescence gradually intensified as SIN-1 stimulation proceeded. These results taken together suggest the sensitivity of **B545b** to image intracellular nitrosative stress.

Next, the selectivity of **B545b** for $ONOO^-$ in live endothelial cells was studied. For this purpose, cells were first treated with $ONOO^-$ scavengers,[36–38] and then were stimulated with SIN-1 or OGD. The results showed that neutralizing $ONOO^-$ with these scavengers significantly decreased SIN-1 or OGD induced **B545b** fluorescence (Fig. 4), suggesting the selectivity of **B545b** for $ONOO^-$ in live cells.

In vivo real-time imaging of the $ONOO^-$ flux incurred by brain microvessel occlusion

Having confirmed the sensitivity and selectivity of probe **B545b** for $ONOO^-$ in live cells, and its good BBB permeability, we then tested its ability to image $ONOO^-$ induced by brain vascular injury in mice. First, a photothrombosis-induced focal ischemia model was used to evaluate its ability to track the $ONOO^-$ flux incurred by brain microvessel occlusion in live mice. For this

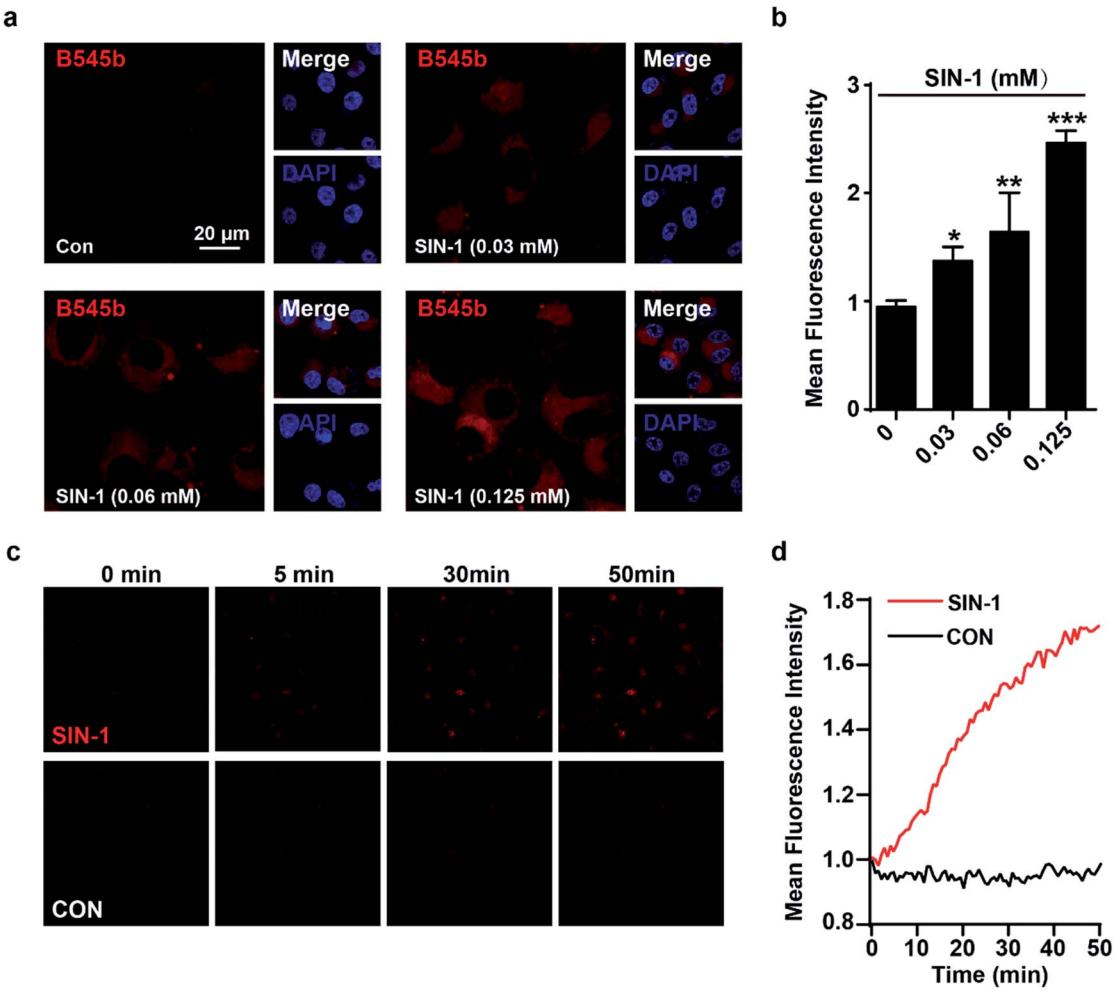

Fig. 3 Imaging SIN-1 induced $ONOO^-$ in EA.hy926 endothelial cells. (a) Cells were incubated with various doses of SIN-1 for 1 h, and then stained with **B545b** (0.5 μM) for 30 min. (b) Quantified **B545b** fluorescence in (a) (mean ± S.E.M, $n = 4$). (c) Time-lapse series of EA.hy926 cells first loaded with **B545b** and then stimulated with SIN-1 (1 mM). (d) Quantified **B545b** fluorescence in (c). Data are presented as a densitometric ratio change compared with control. DAPI (4′,6-diamidino-2-phenylindole) counterstaining indicates nuclear localization (blue, λ_{em} 420–480, λ_{ex} 405 nm). **B545b** fluorescence was collected at 560–620 nm with λ_{ex} 543 nm. ***$P < 0.001$, **$P < 0.01$, and *$P < 0.1$ *versus* control.

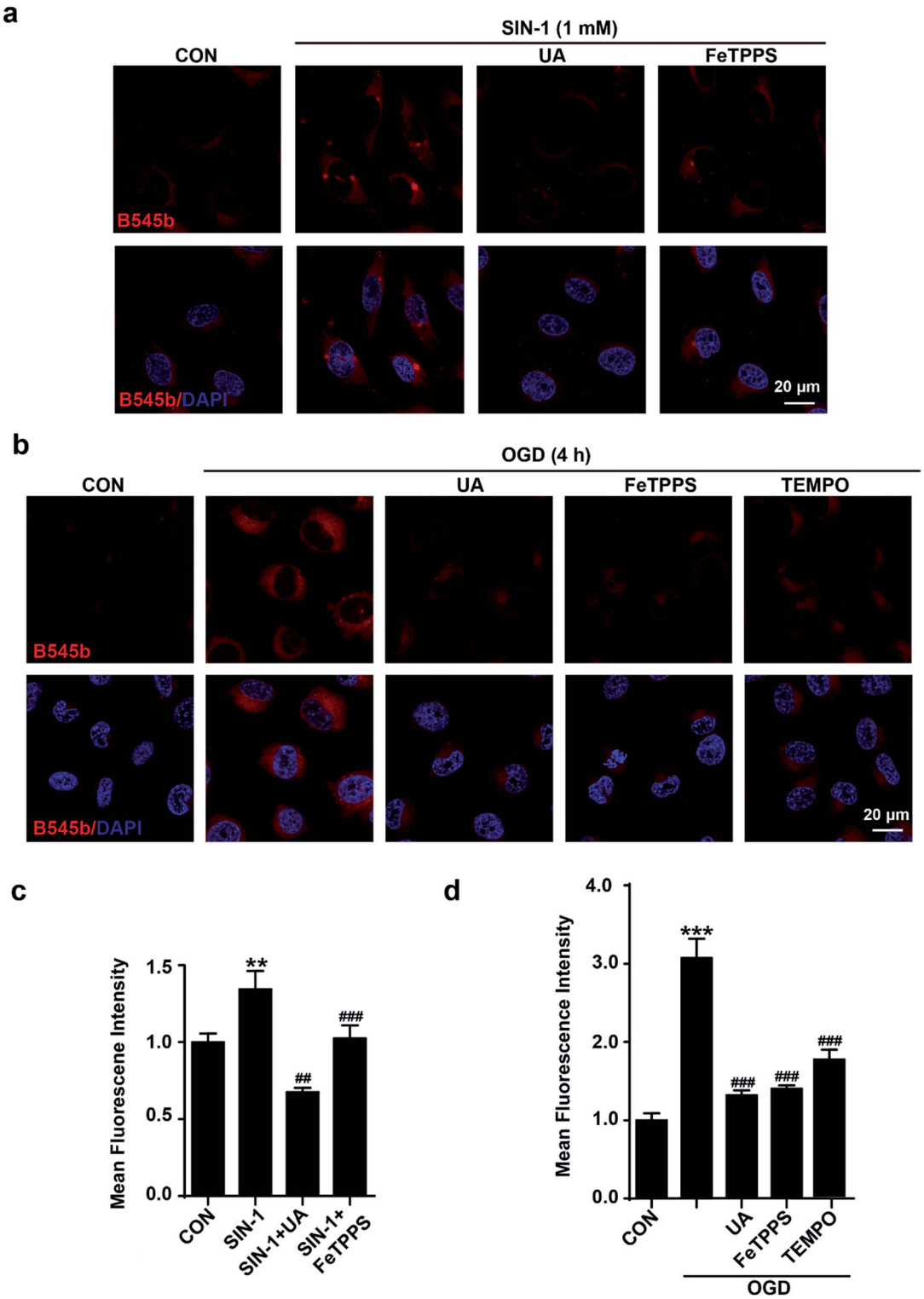

Fig. 4 Characterization of **B545b** specificity for $ONOO^-$ in endothelial cells. (a) Scavenging $ONOO^-$ with uric acid (100 μM) or FeTPPS (1 μM) inhibited SIN-1 induced **B545b** fluorescence. (b) Pretreating cells with uric acid (100 μM), FeTPPS (1 μM) or TEMPO (300 μM) 1 h prior to OGD exposure (4 h) significantly suppressed **B545b** fluorescence. (c and d) Quantification of **B545b** mean fluorescence intensity (mean ± S.E.M, $n = 4$) in (a) and (b). Data are presented as a densitometric ratio change compared with control. DAPI counterstaining indicates nuclear localization (blue, λ_{ex} 405 nm and λ_{em} 420–480 nm). **B545b** fluorescence was collected at 560–620 nm with λ_{ex} 543 nm. ***$P < 0.001$, **$P < 0.01$ *versus* control, ###$P < 0.001$, and ##$P < 0.01$ *versus* SIN-1 or OGD.

purpose, **B545b** was administered to mice through tail injection. One hour later, the mice were subjected to laser irradiation to induce microvessel occlusion and hence ischemic injury.[39] Simultaneously **B545b** fluorescence in the occluded area was recorded using an *in vivo* two-photon laser scanning microscope (TPLSM) (Fig. 5a). As shown in Fig. 5b, which represents the time series of images from a continuous time-lapse movie (S1), **B545b** fluorescence was switched on simultaneously as the intravascular clot occurred, suggesting the immediate overproduction of $ONOO^-$ in response to clot formation. Interestingly, a trace amount of **B545b** fluorescence was also observed around the clotted region once the clot was formed but decreased soon as ischemia progressed, leaving the clotted site which is the major site of $ONOO^-$ overproduction. This result suggests that **B545b** can efficiently detect the burst of pathologic $ONOO^-$ and can visualize the dynamic changes of $ONOO^-$ in a temporally and spatially resolved way. The result also provides the direct proof for the instant overproduction of $ONOO^-$ in vascular injury.

Detecting $ONOO^-$ production in the brain parenchyma after vascular injury

Having confirmed the ability of **B545b** to track the burst of $ONOO^-$ in the clotted microvessel region, we then tested whether it could also detect $ONOO^-$ production in the brain parenchyma after vascular injury. For this purpose, an intraluminal middle cerebral artery occlusion (MCAO) model was used to induce cerebral infarction.[40] Mice were administered with **B545b** through tail injection. 20 min later, the mice were subjected to transient MCAO of 0.5 h or 1 h. An *in vivo* imaging system (IVIS) showed the MCAO-related activation of **B545b** fluorescence in the ipsilateral side of brain 0.5 h after MCAO (Fig. 6a). Ischemic injury evokes a cellular stress response, which involves the expression of FasL. As shown in Fig. 6b, an elevation in FasL expression was observed in MCAO mice, which indicated the damage induced by ischemic injury.[41] Observation of the tissues under a confocal microscope (Fig. 6c) revealed that **B545b** fluorescence increased mainly in the cortex and partly in the striatum of the left brain. There was no significant Nissl staining in the ipsilateral brain at least 0.5 and 1 h after ischemia (Fig. 6d). The control group with **B545b** administration but no MCAO treatment demonstrated negligible **B545b** fluorescence while **B545b** fluorescence was significantly improved in the brain tissues from MCAO-treated mice. This result suggests that a transient ischemia of 30 min, even without reperfusion injury, is sufficient enough to cause nitrosative stress injury to the brain parenchyma. It should be noted

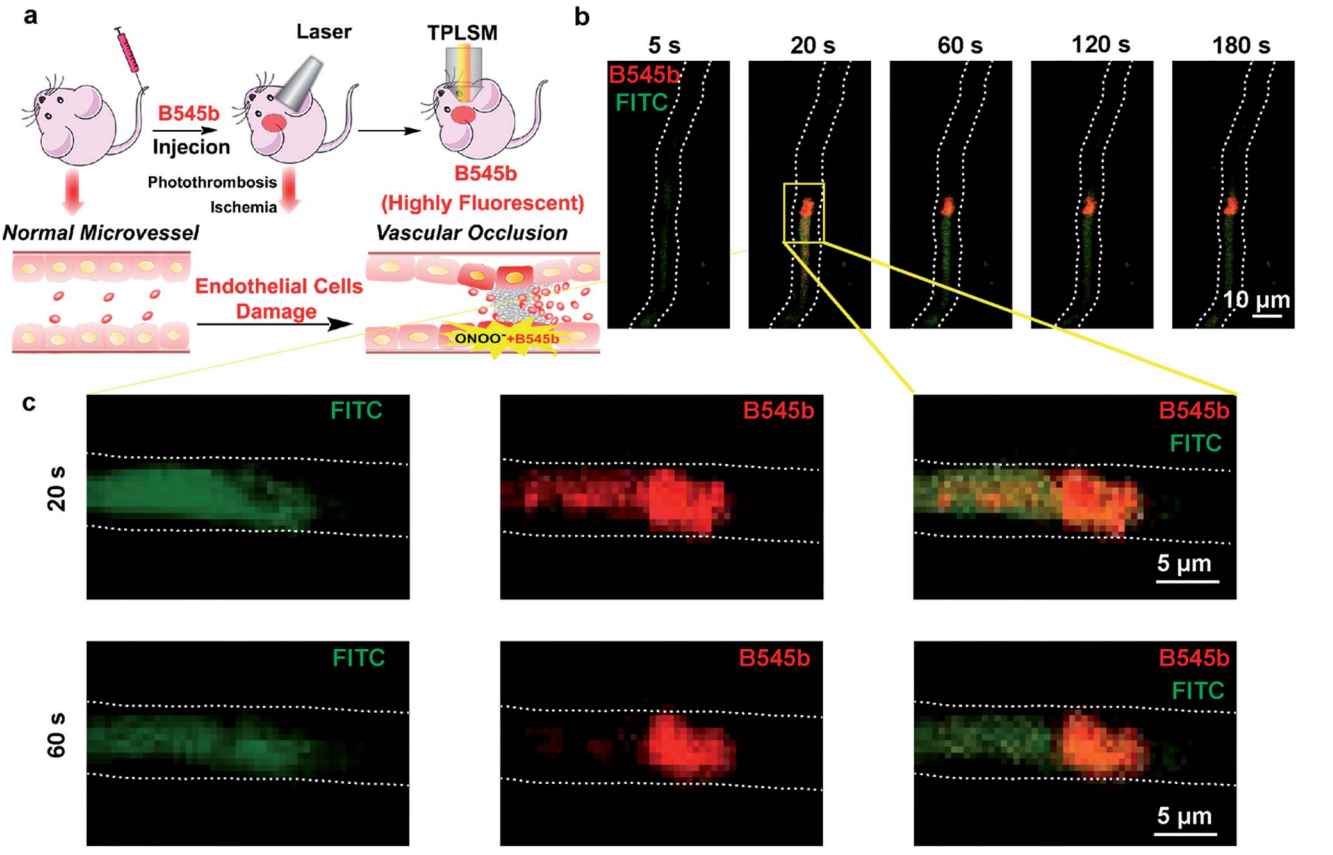

Fig. 5 *In vivo* real-time imaging of the endogenous $ONOO^-$ flux incurred by brain microvessel occlusion. (a) Schematic illustration of experimental methods for microvessel occlusion and imaging. First, probe **B545b** and FITC–dextran were intravenously injected into mice. Then, microvessel occlusion was induced by photothrombosis, and imaged using a two-photon laser scanning microscope (TPLSM). (b) The time-series images representing individual frames from a continuous time lapse movie which showed the dynamic **B545b** fluorescence change in response to vascular occlusion in live mice. (c) Individual fluorescence of **B545b** and FITC in the photothrombosis model.

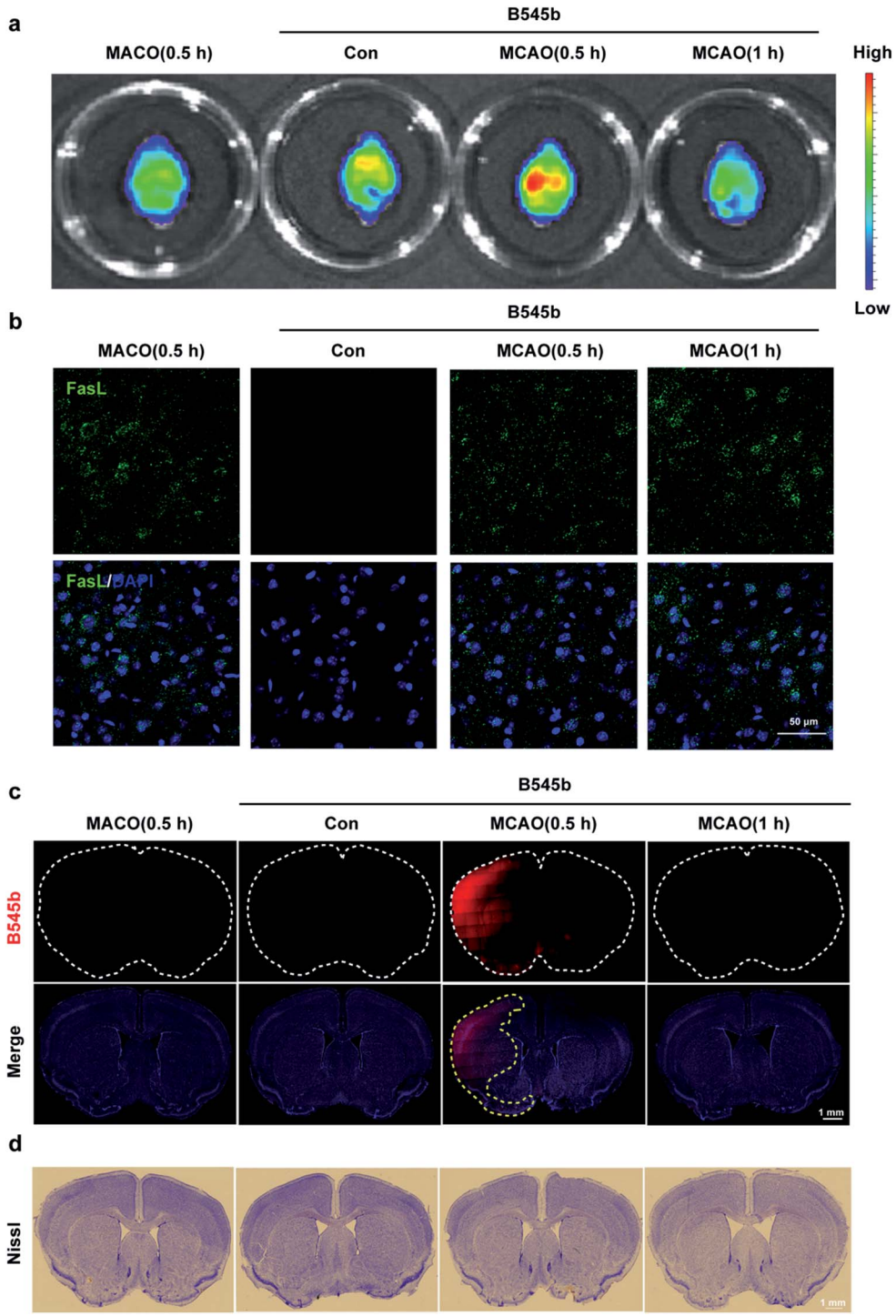

Fig. 6 Imaging of $ONOO^-$ accumulation after MCAO in the brain parenchyma. (a) Cerebral imaging and analysis. After **B545b** administration, the mice were treated with MCAO for 0.5 or 1 h. The whole brains were scanned using a Maestro *in vivo* imaging system with a 480 nm excitation wavelength and a 560 nm filter. (b) Immunofluorescence staining of FasL (green) and DAPI (blue) in the brain after **B545b** injection and MCAO treatment. Scale bar = 50 μm. (c) Confocal imaging of brain slices with the **B545b** signal (red) and DAPI (blue). **B545b** fluorescence was collected at 500–540 nm with λ_{ex} 488 nm. **B545b** fluorescence significantly increased 0.5 h after MCAO in the ischemic brain. The white dotted lines show the brain sections and the yellow dotted lines show the ischemic region of brain. Scale bar = 1 mm. (d) Nissl staining with the whole brain sections. Scale bar = 1 mm.

that an MCAO of 60 min gave weaker **B545b** fluorescence than an MCAO of 30 min, which may be due to the quick metabolism of **B545b**, as shown in Fig S12.†

Conclusions

In summary, using a physicochemical-property guided probe design strategy, we have developed a fluorogenic probe **B545b**

for imaging $ONOO^-$ during the onset of stroke. The probe demonstrates an extremely weak background signal but significant brightness upon $ONOO^-$ stimulation, which makes it sensitive enough to trap endogenously produced pathological $ONOO^-$. Moreover, due to its desirable physicochemical properties including its partition coefficient between water and oil and moderate water solubility, **B545b** can be administered intravenously to mice and it readily penetrates the brain blood barrier. These advantages make **B545b** sensitive enough to track the $ONOO^-$ flux in clotted microvessels, and to image ischemia-induced brain parenchymal damage. Facilitated by **B545b**, immediate $ONOO^-$ overproduction accompanying thrombus formation was observed. Moreover, $ONOO^-$ overproduction in the brain parenchyma was also observed at the early stage of ischemia. This information should be helpful for the design of future anti-oxidant therapy for stroke. These results highlight **B545b** as a promising tool to probe the molecular role of $ONOO^-$ in the progression of neurovascular injury in stroke.

Conflicts of interest

There are no conflicts to declare.

Ethical statement

All animal procedures were performed in accordance with the Guidelines for Care and Use of Laboratory Animals of Zhejiang University and Experiments were approved by the Ethics Committees for Animal Experiments of Zhejiang University.

Acknowledgements

This work was supported in part by the National Natural Science Foundations of China (21778048, 21642007, 81473202, 81573411, and 81225022), the Zhejiang Provincial Natural Science Foundation of China (R18H300001 and Z16H310003), and the National Science & Technology Major Project "Key New Drug Creation and Manufacturing Program" (2018ZX09711002-010-004).

Notes and references

1 G. J. Hankey, *Lancet*, 2017, **389**, 641–654.
2 A. Chamorro, U. Dirnagl, X. Urra and A. M. Planas, *Lancet Neurol.*, 2016, **15**, 869–881.
3 E. H. Lo, M. A. Moskowitz and T. P. Jacobs, *Stroke*, 2005, **36**, 189–192.
4 N. Fukuyama, S. Takizawa, H. Ishida, K. Hoshiai, Y. Shinohara and H. Nakazawa, *J. Cereb. Blood Flow Metab.*, 1998, **18**, 123–129.
5 C. Szabo, H. Ischiropoulos and R. Radi, *Nat. Rev. Drug Discovery*, 2007, **6**, 662–680.
6 A. Chamorro, *J. Stroke*, 2018, **20**, 197–207.
7 S. Amaro, D. Canovas, M. Castellanos, J. Gallego, J. Marti-Febregas, T. Segura and A. Chamorro, *Int. J. Stroke*, 2010, **5**, 325–328.
8 R. Radi, *Proc. Natl. Acad. Sci. U. S. A.*, 2018, **115**, 5839–5848.
9 R. Radi, *J. Biol. Chem.*, 2013, **288**, 26464–26472.
10 J. Chan, S. C. Dodani and C. J. Chang, *Nat. Chem.*, 2012, **4**, 973–984.
11 D. Wu, A. C. Sedgwick, T. Gunnlaugsson, E. U. Akkaya, J. Yoon and T. D. James, *Chem. Soc. Rev.*, 2017, **46**, 7105–7123.
12 D. Cheng, Y. Pan, L. Wang, Z. Zeng, L. Yuan, X. Zhang and Y. T. Chang, *J. Am. Chem. Soc.*, 2017, **139**, 285–292.
13 J. B. Li, L. Chen, Q. Wang, H. W. Liu, X. X. Hu, L. Yuan and X. B. Zhang, *Anal. Chem.*, 2018, **90**, 4167–4173.
14 Y. Wu, A. Shi, Y. Li, H. Zeng, X. Chen, J. Wu and X. Fan, *Analyst*, 2018, **143**, 5512–5519.
15 J. Zhang, X. Zhen, P. K. Upputuri, M. Pramanik, P. Chen and K. Pu, *Adv. Mater.*, 2017, **29**, 1604764.
16 C. Yin, H. Zhu, C. Xie, L. Zhang, P. Chen, Q. Fan, W. Huang and K. Pu, *Adv. Funct. Mater.*, 2017, **27**, 1700493.
17 J. Huang, J. Li, Y. Lyu, Q. Miao and K. Pu, *Nat. Mater.*, 2019, **18**, 1133–1143.
18 D. Cheng, J. Peng, Y. Lv, D. Su, D. Liu, M. Chen, L. Yuan and X. Zhang, *J. Am. Chem. Soc.*, 2019, **141**, 6352–6361.
19 A. J. Shuhendler, K. Pu, L. Cui, J. P. Uetrecht and J. Rao, *Nat. Biotechnol.*, 2014, **32**, 373–380.
20 T. Peng, X. Chen, L. Gao, T. Zhang, W. Wang, J. Shen and D. Yang, *Chem. Sci.*, 2016, **7**, 5407–5413.
21 Y. Li, X. Xie, X. Yang, M. Li, X. Jiao, Y. Sun, X. Wang and B. Tang, *Chem. Sci.*, 2017, **8**, 4006–4011.
22 T. Peng, N. K. Wong, X. Chen, Y. K. Chan, Z. Sun, J. J. Hu, J. Shen, H. El-Nezami and D. Yang, *J. Am. Chem. Soc.*, 2014, **136**, 11728–11734.
23 X. Xie, F. Tang, G. Liu, Y. Li, X. Su, X. Jiao, X. Wang and B. Tang, *Anal. Chem.*, 2018, **90**, 11629–11635.
24 S. A. Hitchcock and L. D. Pennington, *J. Med. Chem.*, 2006, **49**, 7559–7583.
25 K. Setsukinai, Y. Urano, K. Kakinuma, H. J. Majima and T. Nagano, *J. Biol. Chem.*, 2003, **278**, 3170–3175.
26 T. Peng, N. K. Wong, X. Chen, Y. K. Chan, Z. Sun, J. J. Hu, J. Shen, H. El-Nezami and D. Yang, *J. Am. Chem. Soc.*, 2014, **136**, 11728–11734.
27 X. Li, R. R. Tao, L. J. Hong, J. Cheng, Q. Jiang, Y. M. Lu, M. H. Liao, W. F. Ye, N. N. Lu, F. Han, Y. Z. Hu and Y. H. Hu, *J. Am. Chem. Soc.*, 2015, **137**, 12296–12303.
28 T. Peng, X. Chen, L. Gao, T. Zhang, W. Wang, J. Shen and D. Yang, *Chem. Sci.*, 2016, **7**, 5407–5413.
29 K. E. Knewtson, D. Rane and B. R. Peterson, *ACS Chem. Biol.*, 2018, **13**, 2595–2602.
30 D. Li, J. Cheng, C. K. Wang, H. Ying, Y. Hu, F. Han and X. Li, *Chem. Commun.*, 2018, **54**, 8170–8173.
31 T. Rohand, M. Baruah, W. Qin, N. Boens and W. Dehaen, *Chem. Commun.*, 2006, 266–268.
32 A. M. Hakim and E. A. Shoubridge, *Cerebrovasc. Brain Metab. Rev.*, 1989, **1**, 115–132.
33 U. Bickel, *NeuroRx*, 2005, **2**, 15–26.
34 J. H. Jang, O. I. Aruoma, L. S. Jen, H. Y. Chung and Y. J. Surh, *Free Radical Biol. Med.*, 2004, **36**, 288–299.
35 J. Xu, L. He, S. H. Ahmed, S. W. Chen, M. P. Goldberg, J. S. Beckman and C. Y. Hsu, *Stroke*, 2000, **31**, 1744–1751.

36 D. C. Hooper, S. Spitsin, R. B. Kean, J. M. Champion, G. M. Dickson, I. Chaudhry and H. Koprowski, *Proc. Natl. Acad. Sci. U. S. A.*, 1998, **95**, 675–680.
37 T. P. Misko, M. K. Highkin, A. W. Veenhuizen, P. T. Manning, M. K. Stern, M. G. Currie and D. Salvemini, *J. Biol. Chem.*, 1998, **273**, 15646–15653.
38 R. T. Carroll, P. Galatsis, S. Borosky, K. K. Kopec, V. Kumar, J. S. Althaus and E. D. Hall, *Chem. Res. Toxicol.*, 2000, **13**, 294–300.
39 M. Schroeter, S. Jander and G. Stoll, *J. Neurosci. Methods*, 2002, **117**, 43–49.
40 N. Shioda, T. Ishigami, F. Han, S. Moriguchi, M. Shibuya, Y. Iwabuchi and K. Fukunaga, *Neuroscience*, 2007, **148**, 221–229.
41 Y. M. Lu, R. R. Tao, J. Y. Huang, L. T. Li, M. H. Liao, X. M. Li, K. Fukunaga, Z. H. Hong and F. Han, *J. Neuroinflammation*, 2012, **9**, 172.